Published in final edited form as:
J Immunol. 2011 February 15; 186(4): 2127–2137. doi:10.4049/jimmunol.1002878.

Selenoprotein K knockout mice exhibit deficient calcium flux in immune cells and impaired immune responses

Saguna Verma[*,1], **FuKun W. Hoffmann**[†,1], **Mukesh Kumar**[*], **Zhi Huang**[†], **Kelsey Roe**[*], **Elizabeth Nguyen-Wu**[†], **Ann S. Hashimoto**[†], and **Peter R. Hoffmann**[†]

[*]Department of Tropical Medicine, Medical Microbiology and Pharmacology, University of Hawaii, Honolulu, Hawaii U.S.A.

[†]Department of Cell and Molecular Biology, John A. Burns School of Medicine, University of Hawaii, Honolulu, Hawaii U.S.A.

Abstract

Selenoprotein K (Sel K) is a selenium-containing protein for which no function has been identified. We found that Sel K is an endoplasmic reticulum (ER) transmembrane protein expressed at relatively high levels in immune cells and is regulated by dietary selenium. Sel $K^{-/-}$ mice were generated and found to be similar to WT controls regarding growth and fertility. Immune system development was not affected by Sel K deletion, but specific immune cell defects were found in Sel $K^{-/-}$ mice. Receptor-mediated Ca^{2+} flux was decreased in T cells, neutrophils, and macrophages from Sel $K^{-/-}$ mice compare to controls. Ca^{2+}-dependent functions including T cell proliferation, T cell and neutrophil migration, and Fcγ-receptor-mediated oxidative burst in macrophages were decreased in cells from Sel $K^{-/-}$ mice compared to controls. West Nile virus (WNV) infections were performed and Sel $K^{-/-}$ mice exhibited decreased viral clearance in the periphery and increased viral titers in brain. Furthermore, WNV-infected Sel $K^{-/-}$ mice demonstrated significantly lower survival (2/23; 8.7%) compared to WT controls (10/26; 38.5%). These results establish Sel K as an ER-membrane protein important for promoting effective Ca^{2+} flux during immune cell activation and provide insight into molecular mechanisms by which dietary selenium enhances immune responses.

Introduction

Selenium (Se) is an essential micronutrient important for many aspects of human health, including optimal immune responses (1). Both innate and adaptive immunity are impaired in Se-deficient individuals and changes in Se intake affect a range of immune responses including anti-viral immunity, vaccine responses, and allergic asthma (2). Our recent study demonstrated that increased Se intake boosted Ca^{2+} flux and downstream cell signaling in $CD4^+$ T cells, which dramatically influenced their activation, proliferation, and differentiation (3). The biological effects of Se are exerted mainly through its incorporation into selenoproteins as the amino acid, selenocysteine. Twenty-five selenoproteins have been identified in humans, all but one of which also exist as selenocysteine-containing proteins in mice and rats (4). Some selenoproteins such as the glutathione peroxidases and thioredoxin reductases have been functionally characterized as antioxidant enzymes, serving to mitigate damage caused by reactive oxygen species and to regulate redox tone within or outside of

Address correspondence to: Peter R. Hoffmann, University of Hawaii, John A. Burns School of Medicine, 651 Ilalo Street, Honolulu, HI 96813; ph: 808 692-1510; fx: 808 692-1968; peterh@pbrc.hawaii.edu.
[1]S. Verma and F.W. Hoffmann contributed equally to this paper.

There were no conflicts of interests for any of the authors.

cells (5). However, not all selenoproteins act as antioxidant enzymes and functions for several selenoproteins have yet to be determined.

One selenoprotein for which no function has been identified is selenoprotein K (Sel K), which is a small (~12 kDa) protein first identified through a bioinformatic analysis of the human genome (4). Both human and mouse Sel K contain one selenocysteine residue and share 91% amino acid sequence identity. One investigation into potential functions of Sel K showed that its overexpression in cardiomyocytes decreased sensitivity to treatment with hydrogen peroxide (6). However, it was not demonstrated whether endogenous Sel K serves in an antioxidant capacity or potential mechanisms by which this may occur. The *Drosophila melanogaster* ortholog of Sel K was not found to contribute to antioxidant potential in this organism (7). Moreover, Sel K lacks defined redox motifs found in antioxidant selenoproteins like the glutathione peroxidase (GPx) and thioredoxin reductase (TxnRd) enzymes (8). A recent study suggested that Sel K expression in HepG2 cell line is regulated by endoplasmic reticulum (ER) stress and decreasing its expression with siRNA augmented cell death induced with ER stress-inducing agents (9). Whether Sel K is directly or indirectly linked to ER stress in vivo remains unclear.

The Sel K amino acid sequence contains a predicted transmembrane domain, a feature found in only four other selenoproteins: deiodinase 2, and selenoproteins I, N, and S (5). In one study, overexpression of GFP-tagged Sel K resulted in its localization to the ER (6), while other data have suggested that Sel K may localize to the plasma membrane (4). These two different findings may be reconciled by the fact that regions of ER come in close proximity to the plasma membrane (within 10–25 nm), regions commonly referred to as puncta (10). Puncta provide microenvironments in which key signaling events occur between the ER and the plasma membrane, particularly during Ca^{2+} influx and activation of T cells (11). Overall, important questions remain regarding subcellular localization and biological functions of Sel K and more information is needed regarding its in vivo role.

Clues to potential biological roles for Sel K may be obtained by analyzing its tissue distribution. Based on Northern blot analysis, expression of Sel K was suggested to be relatively high in the heart (6). However, real-time RT-PCR data subsequently published by our laboratory demonstrated that Sel K mRNA expression levels are widely distributed throughout most tissues, with particularly high levels detected in spleen and testes (12). An immunohistochemical survey of human tissues suggested relatively high expression in the salivary gland and lymphoid tissues (13). We report in this study that Sel K is an ER-membrane protein expressed at relatively high levels in lymphoid tissues and a variety of immune cells, which raises the question of the role it plays in leukocytes during immune system development and immune responses. To address this issue, Sel $K^{-/-}$ mice were generated and found to be similar to WT controls in terms of immune system development. We found that Sel K deletion impairs receptor-mediated Ca^{2+} flux and Ca^{2+}-dependent functions such as proliferation, chemotaxis, and Fcγ-receptor mediated oxidative burst. Furthermore, Sel $K^{-/-}$ mice exhibited impaired immune responses when infected with West Nile virus (WNV) as demonstrated by decreased viral clearance in periphery, increased viral titers in brain, and increased mortality, suggesting an important role for Sel K in maintaining effective immunity.

Materials and methods

Construction of targeting vector and embryonic stem cell clones

A targeting vector was designed and constructed with inGenious Targeting Laboratory, Inc. (Stony Brook, NY) and included a 11.31 Kb region of the wild-type *sel K* locus sub-cloned from a positively identified C57BL/6 (RPCI23: 227C3) BAC clone. The region was

designed such that the short homology arm (SA) extended approximately 1.53 Kb 5' to exon 2. The long homology arm (LA) terminated 3' to exon 3 and was 7.52 Kb in length. The loxP flanked Neo cassette was inserted on the 5' side of exon 2 and a single loxP site was inserted at the 3' side of exon 3. The target region was 2.27 Kb and included exons 2–3. The total size of the targeting construct, including vector backbone (pSP72, Promega) and Neo cassette, was 15.52 Kb. Ten micrograms of the targeting vector was linearized by NotI and then transfected into iTL1 C1 C57BL/6 embryonic stem cells by electroporation. After selection with G418 antibiotic, surviving clones were expanded and analyzed by PCR to identify recombinant ES clones. Secondary confirmation of positive clones identified by PCR was performed by Southern Blot analysis. DNA was digested with PstI and electrophoretically separated on a 0.8% agarose gel. After transfer to a nylon membrane, the digested DNA was hybridized with a 5' external probe. DNA from C57BL/6 mouse strain was used as a WT positive control.

Generation of Sel K-deficient mice

ES clones were injected into C57BL/6 blastocysts to produce chimeras with one WT and one floxed Sel K allele, Sel $K^{wt/fl}$ mice, which were then mated to generate Sel $K^{fl/fl}$ mice on a C57BL/6 background. FLP1 and CMV-Cre transgenic mice were purchased from the Jackson Laboratory. FLP1 transgenic mice were mated with Sel $K^{fl/fl}$ mice to generate offspring with the Neo cassette excised, which were mated to regenerate Sel $K^{fl/fl}$ mice. These mice were then mated with CMV-Cre transgenic mice to generate offspring in which Sel K was deleted in all tissues (Sel $K^{-/-}$ mice). Excision of Sel K was confirmed in all offspring using PCR that amplified a 408 b.p. product in the targeted region present in the WT allele (fwd: ttc ctg ccc tag ttg agt tct tct; rev: tgt atg cca ttc tta gtc cag ttt) and a 1.6 Kb product in the excised allelle (fwd: cgc ctc cga gaa tta cat act ga; rev: gct ggg gcc acg aag gt). C57BL/6J mice were purchased from the Jackson Laboratory to generate a colony of wild-type mice. In some cases, diets with low (0.08 ppm), medium (0.25 ppm), and high (1.0 ppm) Se were fed for 8 weeks as previously described (3). In all other experiments standard chow (approximately 0.25 ppm Se) was used. All animal experimental protocols were approved by the University of Hawaii Institutional Animal Care and Use Committee.

Antibodies and reagents

Antibodies for flow cytometry included PE-anti-CD3, PE-anti-CD4, APC-anti-CD4, PE-anti-CD11b, APC-anti-CD16/32 (all purchased from Ebioscience); APC/Cy7-anti-CD11b, PerCP-Cy5.5-anti-Gr-1, and PE/Texas Red-anti-B220 (all purchased from BD Pharmingen), PE-anti-F4/80 and Alexa647-anti-CXCR2 (BioLegend). Rabbit polyclonal anti-Sel K purchased from Sigma or custom rabbit polyclonal antibody purchased from Pro-Sci, Inc. were used for Western blots and immunohistochemistry. Mouse monoclonal anti-α-tubulin was purchased from Novus Biologicals, anti-β-actin from Sigma, anti-stromal interaction molecule 1 (STIM1) from Abgent, and both anti-KDEL and anti-Tata Binding Protein (TBP) from Abcam. Rabbit polyclonal anti-Akt was purchased from Cell Signaling. HRP- or fluorochrome-conjugated secondary antibodies were purchased from Jackson Immunolabs or Invitrogen, respectively. Thapsigargin, ionomycin, tunicamycin, and poly (i:c) were purchased from Sigma. Recombinant KC, RANTES, and stromal cell-derived factor 1 (SDF-1) were purchased from R&D Systems.

Preparation of ex vivo cells and flow cytometry

Tissues were homogenized using a Miltenyi gentleMACS cell dissociator. For lymph nodes, two inguinal and two axillary lymph nodes were pooled from each mouse and cell numbers were calculated per lymph node. A Miltenyi cell separation system with appropriate magnetic beads was then used to negatively purify pan T cells, $CD4^+$ T cells, or $CD8^+$ T cells from spleens or to positively purify Gr-1^+ neutrophils from bone marrow. After

washing with RPMI media, cells were resuspended in complete RPMI media and purification confirmed using flow cytometry. For bone marrow-derived macrophages (BMDM), bone marrow was flushed from femurs and tibiae with HBSS using a syringe with a 25-gauge needle. Cells were release from clumps using a syringe with an 18-gauge needle and cell suspensions passed through a 40-μm pore cell strainer (BD Falcon) to remove tissue debris. The cells were then plated in DMEM containing 10% FCS, 1% penicillin/ streptomycin/L-glutamine (Invitrogen), and 5 ng/mL recombinant M-CSF (R&D Systems) and used on day 7 of culture.

Western blotting and immunohistochemistry

Western blots were performed as previously described (12), with slight modifications. To maximize yield of Sel K, tissues and cell pellets were lysed in a low salt buffer containing 10 mM Tris pH 7.5, 1% Triton X-100, 5 mM EDTA, proteinase and phosphatase inhibitors, and 5 mM NaCl. Densitometry was performed using the Li-Cor Odyssey imaging system. A compartment protein extraction kit (Millipore) was used to prepare membrane, nuclear, and cytoplasmic fractions from whole cell lysates. Immunohistochemistry was performed as previously described (14), with modifications including the use of rabbit polyclonal anti-Sel K (ProSci, Inc) as a primary antibody followed by HRP-anti-rabbit IgG.

Oxidative burst assay and bead uptake

IgG-opsonized BSA for Fcγ-receptor-mediated Ca^{2+} flux assays was generated by adding 20 μg BSA (Sigma) with 200 μg rabbit polyclonal anti-BSA (Upstate/MIllipore) and PBS in a final volume of 500 μL. Oxidative burst was determined in a time-course manner using Fc OxyBURST fluorescent assay reagent (Invitrogen) and measured on a FACScaliber (BD Biosciences). For phagoyctosis assays, yellow-green fluorescent, 1 μm carboxylate-modifed FluoSpheres® were purchased from Invitrogen and incubated with BMDM for one hour at 37°C. After washing nonphagocytosed beads, BMDM were fixed with 2% PFA and stained with PE-anti-F4/80 as a plasma membrane fluorescent stain. Confocal images were captured using a Zeiss Axiovert 200M attached to a Zeiss LSM 5 Pascal imaging system and 3-D rendering performed using ImageJ software.

Poly(i:c)-induced peritonitis and cytokine measurement

Each mouse was injected i.p. with 150 μg poly(i:c) in 150 μL PBS and maintained in cages for 48 h to allow infiltration of several different types of innate immune cells. Mice were then sacrificed and a syringe with a 18 g needle was used to inject and withdraw cold complete RPMI media. Cells were centrifuged, washed twice with cold RPMI containing no phenol red, and resuspended in cold FACS buffer (PBS with 2% FBS). Four-color flow cytometry was then performed on cell samples from each peritoneal lavage as previously described (15). Also, serum was collected from each mouse and analyzed by Cytometric Bead Array and Flexibead kits (BD Biosciences) per manufacturer's instructions.

ER-stress measurement

To determine levels of ER-stress, an established protocol (16) was followed using conventional RT-PCR and Pst I digestion to determine relative levels of spliced and unspliced X-box-binding protein-1 (XBP-1). Primers used to amplify XBP-1 included fwd: 5'-A AAC AGA GTA GCA GCG CAG ACT GC-3' and rev: 5'-TC CTT CTG GGT AGA CCT CTG GGA G-3' and PCR conditions included 94°C for 4 min, 35 cycles of 94°C for 10 s, 66°C for 30 s, and 72°C for 30 sec, followed by 72°C for 10 min final extension. Tunicamycin was added as a control to induce ER-stress at 5 μg/mL for 7 h. ER-stress was also determined by western blot analysis of BiP (Grp78;) using whole cell lysates from spleen or BMDM cells untreated or treated with tunicamycin for 24 h.

Calcium Flux and Migration Assays

Purified T cells or neutrophils were loaded with Fluo3/AM and FuraRed (3 μM and 3.3 μM, respectively; Invitrogen) for 30 min at RT in RPMI with no FBS. Following two washes with complete RPMI, cells were resuspended in complete RPMI with no phenol red and Ca^{2+} flux assays performed by measuring the ratio of Fluo3 (FL-1) to FuraRed (FL-3) fluorescence on a FacsCaliber as previously described (17). Migration assays were performed using CytoSelect 24-well Cell Migration Assay kits (Cell Biolabs, Inc.). For neutrophils, 1.5×10^6 cells in 300 μL serum-free media were added to the upper chamber of the transwell plates with 3 μm pore-size filters. Lower chambers contained 500 μL RPMI media and varying concentrations of KC and migration carried out for 2.5 h at 37°C and 10% CO_2. For T cells, 10^6 cells in 200 μL serum-free media were added to the upper chamber of transwell plates with 5 μm pore-size filters. Lower chambers contained 500 μL RPMI media with varying concentrations of either RANTES or SDF-1 and migration carried out for 3.5 h at 37°C and 10% CO_2. The number of cells migrating to lower chambers was determined by fluorescence per manufacturer's instructions on a Victor 2 plate reader (Perkin Elmer, Inc.). For macrophages, BMDM were grown on glass coverslips and loaded with fluorescent Ca^{2+} indicator dye Fluo-4/AM (Invitrogen) at 5 μM for 30 min followed by washes and covered with complete DMEM with no phenol red. Cells were mounted in a rapid-exchange Warner perfusion system for confocal imaging using a Zeiss Axiovert 200M attached to a Zeiss LSM 5 Pascal imaging system. Fluo4 signal was quantitatively analyzed using NIH Image-J software.

Proliferation assays

Proliferation of T cells was measured using ^{3}H-thymidine techniques by plating 5×10^5 cells in 200 μl per well in a 96-well plate pre-coated with anti-CD3 (1 ug/ml) plus anti-CD3/28 (10 ug/ml). Cells were incubated for 72 h in RPMI containing 10% FBS. For the last 18 h, a master mix containing 0.5 ul ^{3}H-thymidine/well (spec. act. 25 Ci/mol, radioactive conc. 1.0 mCi/ml, Amersham [methyl-^{3}H]) was added to each well. Cells were harvested using a Skatron Instruments Semiautomatic Cell Harvester (Lier, Norway) and levels of isotope incorporated into DNA measured using a Packard Bioscience/Perkin Elmer Tri-Carb 2900TR liquid scintillation counter (Waltham, MA).

WNV infections, plaque assays, and RT-PCR

All infection experiments were performed using the lineage I WNV strain (NY99) and in accordance with the guidelines of the University of Hawaii's Animal Care and Use Committee. For survival studies, male and female mice between 10–12 wk of age maintained on normal mouse chow (approximately 0.25 ppm Se) were inoculated via the footpad route with 10^2 PFU WNV and the disease symptoms and mortality was observed for 18 days. On days 3 and 6, 100 – 200 μL blood was collected from tail-veins, from which sera was separated and frozen for subsequent analyses. WNV replication in the sera was analyzed by plaque assay using Vero cells as previously described (18, 19). For quantitation of viral burden in the brain at day 7 after infection, separate group of mice were perfused with 10 to 15 mL of phosphate buffered saline, whole brains harvested, tissue homogenized and total RNA was extracted using RNeasy kit (Qiagen). WNV copy number was quantitated using quantitative real-time RT-PCR (qRT-PCR) analyses using a WNV-specific probe as previously described (18, 19).

Statistical Analyses

Comparison of means was carried out using an unpaired Student's t test (parametric test) or Mann-Whitney (non-parametric test) using GraphPad Prism version 4.0. For survival

analyses, Prism 4.0 was used to perform a Kaplan-Meier log-rank test to compare curves. All comparisons were considered significant at $P < 0.05$.

Results

Sel K is an ER-localized, membrane protein expressed in immune tissues and cells that is regulated by dietary Se levels

Data describing the relative levels of Sel K mRNA in different tissues have been conflicting (6, 12), and limited information is available regarding Sel K protein expression. To assess Sel K tissue distribution in mice, western blot analysis of eight tissues was performed and results demonstrated relatively high expression of Sel K in spleen and, to a lesser extent, in intestine (Fig. 1A). Western blot analyses also detected Sel K protein in several different types of human and mouse immune cells (Fig. 1B). Some selenoproteins are more sensitive to changes in dietary Se in terms of expression levels (20). So, we examined spleens of mice fed diets with low (0.08 ppm), medium (0.25 ppm, which is equivalent to levels in standard chow), and high (1.0 ppm) Se levels and found that Sel K expression was significantly decreased in the mice fed low Se (Fig. 1C). The effects of increased Se intake on Sel K expression was similar to that observed for western blot analysis of GPx1 (Fig. S1[δ]) and both GPx and Txnrd activities (3). Also, higher dietary Se (1.0 ppm) increased Sel K expression to detectable levels in most tissues examined except for heart (Fig. S2). Although the Sel K amino acid sequence contains a predicted transmembrane domain, no data are available confirming membrane localization. Subcellular fractionation of Jurkat T cells was performed followed by western blotting and Sel K was detected only in the membrane fraction (Fig. 1D). Fluorescent microscopy revealed that endogenous Sel K localized to the ER in human lymphocytes (Fig. 1E), which is consistent with previous data showing that overexpressed, GFP-tagged Sel K localized to the ER in HEK293 cells (6). Moreover, Sel K was detected by immunohistochemistry in mouse lymph nodes and exhibited a perinuclear distribution consistent with ER localization (Fig. 1F and S3). Taken together, these results suggest that Sel K is an ER-membrane protein expressed at relatively high levels in immune cells and is regulated by dietary Se levels.

Sel K-deficient mice are healthy with normal immune system development

Sel K-deficient mice were generated using a conditional knockout approach due to the possibility that conventional knockout of Sel K may be embryonic lethal. Mice were generated with loxp sites flanking exons 2 and 3 of the Sel K gene on a C57BL/6 genetic background and crossed with CMV-Cre mice to produce offspring with Sel K deleted in all tissues (Fig. 2A). Excision of the targeted region of the Sel K gene was confirmed by PCR (Fig. 2B) and Sel K protein was undetectable and in all tissues examined from Sel $K^{-/-}$ mice, including spleen (Fig. 2C).

Sel $K^{-/-}$ mice were born at the expected Mendelian ratio and developed normally to adulthood. Sel $K^{-/-}$ mice were fertile and showed no differences from WT mice in terms of weight gain, although no detailed analyses have yet been performed to fully characterize metabolism in these mice. Because of the relatively high levels of Sel K expressed in lymphoid tissues such as thymus, lymph nodes, and spleen (Fig. 1 and S4), immune system development was examined in the knockout mice. Compared to WT controls, Sel $K^{-/-}$ mice exhibited no differences in cell numbers in lymphoid tissues (Table I), suggesting that immune system development was not affected by Sel K deletion. Also, percentages of myeloid and lymphoid cells in liver and lung were similar between WT and Sel $K^{-/-}$ mice (data not shown). Overall, Sel K deletion appeared to have no overt effect on the phenotype

[δ]The online version of this article contains supplemental material

of the mice including immune system development and immune cell populations in peripheral tissues.

Sel K-deficient T cells, neutrophils, and macrophages exhibit decreased receptormediated calcium flux

Our finding that Sel K is a transmembrane protein localized to the ER of immune cells was of interest because the ER is the key site for initiation of store-operated Ca^{2+} entry (SOCE) during of immune cell activation (21). Thus, we analyzed SOCE by measuring intracellular Ca^{2+} levels during activation of T cells, neutrophils, and macrophages from WT and Sel $K^{-/-}$ mice. Activation through the TCR induced lower Ca^{2+} flux in T cells from Sel $K^{-/-}$ mice compared to WT controls (Fig. 3A). Also, Ca^{2+} flux was reduced in response to two chemokines, RANTES and SDF-1, in T cells from Sel $K^{-/-}$ mice compared to WT controls (Fig. 3B–C). Similarly, stimulation of neutrophils with the chemokine, KC, resulted in lower Ca^{2+} flux in neutrophils from Sel $K^{-/-}$ mice compared to WT controls (Fig. 3E). BMDM were analyzed for Ca^{2+} flux induced by engagement of Fcγ-receptors using IgG-opsonized BSA, and results demonstrated that Ca^{2+} flux was significantly decreased in Sel $K^{-/-}$ BMDM compared to WT controls (Fig. 3G). For all three cell-types examined, Sel K deletion did not affect Ca^{2+} flux induced by thapsigargin, which inhibits sarco/endoplasmic reticulum Ca^{2+} ATPases and non-specifically releases Ca^{2+} from ER stores causing Ca^{2+} to enter through calcium release-activated Ca^{2+} (CRAC) channels in the plasma membrane (Fig. 3D, F, and H). This suggests that Sel K deletion does not affect levels of Ca^{2+} stored in the ER or Ca^{2+} influx at the level of plasma membrane CRAC channels. The Ca^{2+} ionophore, ionomycin, was added as a control at the end of these experiments to open Ca^{2+} channels and intracellular stores on top of that already mobilized by the previous stimuli. KO cells did not differ from WT in fluorescence by an amount more than the difference from the first stimuli for all three cell-types, suggesting the KO cells were healthy and able to flux Ca^{2+} in response to this ionophore. We also examined the possibility that Sel K deletion may cause ER-stress in these cells, which may lead to generalized ER dysfunction. However, there were no differences in ER-stress markers between WT and Sel $K^{-/-}$ spleen cells or BMDM (Fig. S5). Overall, Sel K deletion does not affect the ability of the ER to induce SOCE in a general manner, but specifically impairs receptor-mediated ER Ca^{2+} flux.

Sel K-deficient T cells exhibit decreased proliferation and migration

Because Ca^{2+} flux was impaired in T cells from Sel $K^{-/-}$ mice and Ca^{2+} flux is important for T cell proliferation, we analyzed the effect of Sel K-deficiency on the proliferative capacity of T cells. Proliferation was decreased in both $CD4^+$ and $CD8^+$ T cells from Sel $K^{-/-}$ mice compared to WT controls (Fig. 4A). Proliferation was only partially diminished (15% and 20% decrease for $CD4^+$ and $CD8^+$ T cells, respectively), but the decreases were statistically significant. T cell migration induced through chemokine receptors also requires efficient Ca^{2+} flux (22), and this function was measured in response to two T cell chemokines, SDF-1 and RANTES. Migration in response to both chemokines was significantly decreased in Sel $K^{-/-}$ T cells compared to WT controls (Fig. 4B–C). Interestingly, migration from upper to lower chambers in absence of either chemokine was also decreased in Sel $K^{-/-}$ T cells, suggesting an effect of Sel K deletion on passive migration through the transwell pores.

Sel K-deficient neutrophils exhibit reduced migration

Similar to T cells, chemotaxis of neutrophils depends on efficient Ca^{2+}-release from ER upon chemokine receptor engagement (23, 24). To determine if neutrophils from Sel $K^{-/-}$ or WT mice demonstrated differences in chemotactic capacity, migration assays were performed using neutrophils purified from bone marrow of these mice. The frequency of neutrophils in bone marrow and expression of the chemokine receptor for KC, CXCR2,

were similar between WT and Sel $K^{-/-}$ mice (Fig. 5A). However, when these cells were purified and tested for their ability to migrate in response to KC, migration was significantly decreased in neutrophils from Sel $K^{-/-}$ mice compared to WT controls (Fig. 5B).

To test the in vivo effect of Sel K deletion on neutrophil migration, peritonitis was induced in WT and Sel $K^{-/-}$ mice using i.p. injection of a viral mimetic, poly(i:c), and cellular infiltration was analyzed. Although no differences were found in total cellular infiltration, Gr-1^+ neutrophil influx was slightly decreased in Sel $K^{-/-}$ mice (Fig. 6A–B). Other innate cell types did not differ significantly, including monocytes/macrophages ($CD11b^+$), dendritic cells ($CD11c^+$), and NK cells ($NK1.1^+$). Importantly, no differences were found between KO and WT in terms of leukocytes circulating in blood, including Gr-1^+, $CD11b^+$, $CD3^+$, and $B220^+$ cells (Fig. S6). This supports the notion that lower neutrophil populations in the inflamed peritoneal tissue of KO were not due to lower frequency of circulating cells, but to impaired migration of these cells. Sera from these mice were analyzed for levels of TNFα, MCP-1, IL-6, IL10, IL-12p70, IFNγ, and KC. Of these cytokines, three were detectable: TNFα, MCP-1, and KC (Fig. 6C). Decreased levels of MCP-1 and KC were detected in Sel $K^{-/-}$ mice compared to WT controls, while TNFα levels did not differ. Thus, the infiltration of neutrophils as well as the production of chemokines important for inducing their infiltration were impaired in Sel $K^{-/-}$ mice during peritonitis.

Sel K-deficient macrophages exhibit reduced Fcγ-receptor-mediated oxidative burst

An important function of macrophages during immune responses is the efficient phagocytosis and elimination of IgG-opsonized pathogens through Fcγ-receptor-mediated oxidative burst, which is dependent on effective Ca^{2+} flux (25). To determine the effect of Sel K-deficiency on Fcγ-receptor-mediated oxidative burst, we performed a time-course experiment using BMDM from Sel $K^{-/-}$ and WT mice. Despite similar levels of Fcγ receptors (CD16/32) on their cell surfaces, Sel $K^{-/-}$ BMDM produced a significantly lower Fcγ-receptor-mediated oxidative burst compared to WT controls (Fig. 7A–B). Importantly, phagocytosis in general was not impaired in BMDM from Sel $K^{-/-}$ mice as determined by polystyrene bead uptake (Fig. 7C). TLR-induced cytokine production is another function that has been suggested to depend on Ca^{2+} flux, although the data are limited (26). BMDM from Sel $K^{-/-}$ and WT mice were analyzed for production of pro-inflammatory cytokines TNFα, MCP-1, IL-6, IL-12p70, and IFNγ in response to two TLR agonists: LPS and poly (i:c). Results demonstrated that of the three cytokines that were secreted by BMDM (MCP-1, IL-6, and TNFα), only IL-6 and TNFα were significantly diminished in Sel $K^{-/-}$ BMDM compared to WT controls (Fig. S7). Overall, Sel K deletion selectively affected the functions of BMDM that require Ca^{2+} flux including Fcγ-receptor-mediated oxidative burst and TLR-induced secretion of select cytokines.

Viral infection of Sel K-deficient mice leads to inadequate viral clearance and increased mortality

Proper activation and migration of host immune cells is required for effective immune responses to pathogens, and the importance of these immune functions is particularly evident in experiments involving the mouse model of WNV infection. Inadequate WNV clearance in the periphery due to diminished or defective immune responses leads to increased WNV invasion into central nervous system tissue, and higher mortality due to higher numbers of infected neurons (27). Sel $K^{-/-}$ and WT mice were infected with 10^2 PFU of WNV in the footpad and analyzed for survival and viral clearance. As shown in Fig. 8A, survival was significantly reduced in Sel $K^{-/-}$ mice (2/23,8.7%) compared to WT controls (10/26, 38.5%). To understand how Sel K deletion increased susceptibility to WNV infection, levels of WNV titers were determined by plaque assay and qRT-PCR in sera and brain, respectively. At day 1 post-infection, WNV titers in sera were below detectable levels

(data not shown) and then peaked at day 3 in both WT and Sel $K^{-/-}$ (Fig. 8B). At day 6 post-infection, WNV titers were lower than day 3 for both WT and Sel $K^{-/-}$, but significantly higher levels of WNV were detected in Sel $K^{-/-}$ sera compared to WT controls. Also, WNV titers were higher (by 1.5 $\log_{10}$ PFU) in brains from Sel $K^{-/-}$ at day 7 compared to WT controls (Fig. 8C). Immune responses to WNV depend on anti-viral cytokines produced by immune cells in the periphery to limit neuroinflammation that may lead to death (27). Compared to WT mice, KO mice exhibited decreased levels of key cytokines in sera suggesting impaired anti-WNV immunity while neuroinflammation was increased as determined by brain tissue cytokines and histological evaluation (Fig. 8D and S8). Thus, Sel $K^{-/-}$ mice exhibited increased WNV load in the periphery followed by increased viral load in the brain, which coincided with the onset of increased neuroinflammation, neurodegeneration, and mortality compared to WT controls.

Discussion

No in vivo roles have been revealed for Sel K since the identification of the Sel K gene in 2003 (28). An initial clue to potential functions for Sel K was our finding that this protein is expressed at relatively high levels in lymphoid tissues and immune cells. To our knowledge, this is the first evidence of a selenoprotein exhibiting enriched expression in immune cells or tissues. Higher expression in lymphoid tissues combined with its localization to the ER-membrane in immune cells suggests Sel K may serve a particularly important role in immune cell activation. Using a novel Sel $K^{-/-}$ mouse model, Sel K was clearly demonstrated to be involved in promoting efficient Ca^{2+} flux during activation of immune cells such as T cells, neutrophils, and macrophages. Ca^{2+} flux induced during activation of other immune cells such as B cells is possible given that we detected Sel K expression in primary B cells. Future studies will determine if B cells, mast cells, and other immune cells required Sel K for activation dependent on efficient Ca^{2+} flux.

Although Ca^{2+}-dependent functions were impaired in immune cells from Sel K-deficient mice, many functions were only partially impaired. For example, T cell proliferation was only partially decreased (15 – 20%), whereas T cell migratory capacity was effectively eliminated. Ex vivo neutrophil migration in response to high doses of KC (10 ng/mL) or in vivo migration during peritonitis were only partially decreased. Finally, the peak Fcγ-receptor-mediated oxidative burst was significantly reduced in Sel $K^{-/-}$ macrophages, but only by 33%. Thus, these functions do not entirely depend on the expression of Sel K and suggest a supportive role for this selenoprotein in promoting Ca^{2+}-dependent immune cell functions. In this sense, Sel K should not be considered a limiting factor during Ca^{2+}-dependent signaling and more likely serves to coordinate or facilitate Ca^{2+} flux during immune cell activation.

The role of Sel K in Ca^{2+}-dependent activation of immune cells may provide important insight into the mechanisms by which dietary Se enhances immunity. Our recent study demonstrated that increased dietary Se led to increased TCR-induced Ca^{2+} flux in $CD4^+$ T cells (3). Increased cellular Ca^{2+} and has been shown to be an indispensable step in T cell proliferation (29) (30), and the ER is the main Ca^{2+} store in T cells and other immune cells (31). Activation of T cells through the T cell receptor initiates release of Ca^{2+} from this organelle, which subsequently activates CRAC channels in the plasma membrane (32–34). Although our data suggest a role for Sel K in promoting Ca^{2+} flux and the subsequent signaling events in immune cells that rely on this Ca^{2+} flux, the exact mechanism by which Sel K may carry out this function remains unknown. The Sel K amino acid sequence does not contain motifs for canonical Ca^{2+}-binding domains such as EF-hands, epidermal growth factor (EGF)-like repeats, cadherin repeats, or thrombospondin repeats (35, 36). Thus, it is unlikely that Sel K is directly involved in fluxing Ca^{2+} or sensing loss of Ca^{2+} from ER

stores in a manner similar to another ER transmembrane protein, stromal interaction molecule 1 (37). Sel K may act in a more indirect manner to coordinate or facilitate Ca^{2+} flux through protein-protein interactions with signaling molecules, other ER-membrane proteins, or cytoskeleton proteins. For example, the cytoplasmic region of Sel K has a predicted rigid structure that includes several proline residues, with two canonical SH3-binding sequences (R/K-X-X-P-X-X-P-) (38). SH3 domains are present in a variety of cytoplasmic proteins that serve a scaffolding function to promote protein-protein interactions. This suggests that some or all of the functions of Sel K may involve interactions with SH3 domain-containing proteins and formation of protein complexes. Structure/function studies are currently underway to determine how the SH3-binding domain of Sel K may affect Ca^{2+} flux and potential binding partners for Sel K.

Sel K is not the only selenoprotein localized to the ER. In fact, there are five other ER-localized selenoproteins, two of which are located in the ER-membrane (Sel N and Sel S). Sel N has been demonstrated to participate in protein-protein interactions with the ryanodine receptor (RyR), which is a major component of the RyR intracellular Ca^{2+} release pathway (39). However, the RyR system is not utilized by immune cells for SOCE and Sel N appears to regulate RyR-mediated Ca^{2+} mobilization required for normal muscle development and differentiation (5). Sel S is widely expressed in a variety of tissues and has been suggested to participate in the removal of misfolded proteins from the ER lumen for degradation and regulate ER-stress-induced apoptosis (40). Sel K has been suggested to play a similar role (9). Our data suggest that ER-stress is not the mechanism by which Sel K deletion leads to impaired immune cell activation. However, Sel K may play a role similar to Sel S in regulating ER stress in immune and non-immune cells, and knocking out Sel K may not produce detectable ER stress due to redundancy with Sel S. In this sense, Sel K may serve a common role to alleviate ER stress in most cells that requires low abundance, but play an additional Ca^{2+} flux-related role in immune cells. A better understanding of the roles Sel K, Sel N, and Sel S play in the ER-membrane in different cells and tissues warrants further investigation.

Several different types of immune cells are affected by Sel K-deficiency and the cummulative effect of deleting Sel K is an immuno-compromised host. In both humans and mice, increased susceptibility to WNV neuro-invasive disease is correlated with depressed immunity (41). Humoral and cell-mediated responses are important in restricting WNV infection in the periphery, as both B-cell- and T-cell-deficient mice showed significantly higher viral burden and lethality (42–44). Our data reflect a similar pattern, with Sel $K^{-/-}$ mice exhibiting higher viral burden in periphery and brain accompanied by increased mortality, thereby suggesting inadequate viral clearance by the immune system. However, it must also be considered that Sel K-deficiency may increase WNV replication or WNV-induced mortality through mechanisms that do not involve impaired immunity. For example, it is possible that Sel K deletion leads to increased viral replication in infected cells. However, given the decreased ex vivo functions found in both innate and adaptive immune cells, the more likely explanation is that Sel $K^{-/-}$ mice are immuno-compromised. Less robust immune responses, both innate and adaptive immunity, have been demonstrated in Se-deficient animals (2). A particularly important role for sufficient dietary Se intake has been demonstrated for protecting against viral infection, including H3N2 and H1N1 influenza, HIV-1, and coxsackievirus (45–48). It would be of interest to test different infectious disease models on various selenoprotein knockout mice to determine which selenoproteins are important for protecting against different pathogens.

Our results demonstrated a specific effect of Sel K-deficiency on macrophage secretion of cytokines using ex vivo BMDM. Both IL-6 and TNFα were decreased in Sel $K^{-/-}$ BMDM, but not MCP-1. These results differ from those obtained with in vivo injection of poly(i:c),

which did not produce detectable levels of serum IL-6 and showed similar TNFα levels in WT and KO mice. These differences may be due to the times at which cytokines were measured and time-course experiments for different cell types responding to different TLR agonists would better reveal differences between WT and KO cells. Also, receptor uptake of secreted cytokine may dramatically differ between in vivo and ex vivo conditions, contributing to differences measured in each scenario. Another important issue involves the finding with T cell migration wherein Sel $K^{-/-}$ T cells migration was decreased compared to WT even in the absence of chemokines. This suggests that other factors in addtion to chemokine-induced Ca^{2+} flux may be affected by Sel K-deficiency, including adhesion molecule expression or cellular cytoskeleton organization required for cellular movement. Also, our in vivo experiments involving the TLR3 agonist, poly (i:c), revealed both decreased migration and decreased production of chemokines that attract these cells from the circulating blood in KO compared to WT mice. Activation of cells induced by TLR agonists has been shown to depend on effective Ca^{2+} flux (26) and this results in decreased chemokine production. Further investigation into the role that Sel K and Ca^{2+} flux in general play in chemokine production is warranted. Also, it is interesting that TNF was not affected by Sel K-deletion in the in vivo or ex vivo experiments, while other cytokines or chemokines were decreased. This suggests that TNF secretion does not depend on effect Ca^{2+} flux to the same degree as other cytokines or chemokines.

Overall, our results involving a novel Sel K-deficient mouse model establish this selenoprotein, for which no function has yet been described, as important for immune system function. Sel K is required for effective Ca^{2+} flux during immune cell activation and Sel K deletion in mice leads to insufficient immune responses. Our finding that Sel K is important for Ca^{2+}-dependent immune cell functions opens a new field of biological inquiry into molecular mechanisms of Se in enhancing immune responses. Sel K may also prove an effective target of therapeutic modulation of immunity. It is important to consider that Sel K may play other roles not associated with Ca^{2+} signaling and these roles may be important in a wide variety of cells and tissues. This seems likely given that Sel K is slightly detectable, but consistently expressed in non-immune cells and tissues that do not utilize SOCE for activation. Further studies involving Sel K structure and function are currently underway and will allow a better understanding of the role this selenoprotein plays in immune responses and other biological roles.

Supplementary Material

Refer to Web version on PubMed Central for supplementary material.

Acknowledgments

We thank Janet Meeks and Stephanie Lum for their assistance with WNV work.

This research was supported by NIH grants R21AT004844 and R01AI089999. The content is solely the responsibility of the authors and does not necessarily represent the official views of the NCCAM, NIAID, or NIH. The work was also supported by NIH grants G12RR003061 and P20RR016453.

References

1. Rayman MP. Selenoproteins and human health: insights from epidemiological data. Biochim Biophys Acta. 2009; 1790:1533–1540. [PubMed: 19327385]
2. Hoffmann PR, Berry MJ. The influence of selenium on immune responses. Mol Nutr Food Res. 2008

3. Hoffmann FW, Hashimoto AC, Shafer LA, Dow S, Berry MJ, Hoffmann PR. Dietary selenium modulates activation and differentiation of CD4+ T cells in mice through a mechanism involving cellular free thiols. J Nutr. 2010; 140:1155–1161. [PubMed: 20375261]
4. Kryukov GV, Castellano S, Novoselov SV, Lobanov AV, Zehtab O, Guigo R, Gladyshev VN. Characterization of mammalian selenoproteomes. Science. 2003; 300:1439–1443. [PubMed: 12775843]
5. Reeves MA, Hoffmann PR. The human selenoproteome: recent insights into functions and regulation. Cell Mol Life Sci. 2009
6. Lu C, Qiu F, Zhou H, Peng Y, Hao W, Xu J, Yuan J, Wang S, Qiang B, Xu C, Peng X. Identification and characterization of selenoprotein K: an antioxidant in cardiomyocytes. FEBS Lett. 2006; 580:5189–5197. [PubMed: 16962588]
7. Morozova N, Forry EP, Shahid E, Zavacki AM, Harney JW, Kraytsberg Y, Berry MJ. Antioxidant function of a novel selenoprotein in Drosophila melanogaster. Genes Cells. 2003; 8:963–971. [PubMed: 14750951]
8. Lobanov AV, Hatfield DL, Gladyshev VN. Eukaryotic selenoproteins and selenoproteomes. Biochim Biophys Acta. 2009
9. Du S, Zhou J, Jia Y, Huang K. SelK is a novel ER stress-regulated protein and protects HepG2 cells from ER stress agent-induced apoptosis. Arch Biochem Biophys.
10. Wu MM, Buchanan J, Luik RM, Lewis RS. Ca2+ store depletion causes STIM1 to accumulate in ER regions closely associated with the plasma membrane. J Cell Biol. 2006; 174:803–813. [PubMed: 16966422]
11. Luik RM, Wu MM, Buchanan J, Lewis RS. The elementary unit of store-operated Ca2+ entry: local activation of CRAC channels by STIM1 at ER-plasma membrane junctions. J Cell Biol. 2006; 174:815–825. [PubMed: 16966423]
12. Hoffmann PR, Hoge SC, Li PA, Hoffmann FW, Hashimoto AC, Berry MJ. The selenoproteome exhibits widely varying, tissue-specific dependence on selenoprotein P for selenium supply. Nucleic Acids Res. 2007; 35:3963–3973. [PubMed: 17553827]
13. Berglund L, Björling E, Oksvold P, Fagerberg L, Asplund A, Szigyarto CA, Persson A, Ottosson J, Wernérus H, Nilsson P, Lundberg E, Sivertsson A, Navani S, Wester K, Kampf C, Hober S, Pontén F, Uhlén MA. Gene-centric human protein atlas for expression profiles based on antibodies. Mol Cell Proteomics. 2008; 10:2019–2027. [PubMed: 18669619]
14. Hoffmann PR, Kench JA, Vondracek A, Kruk E, Daleke DL, Jordan M, Marrack P, Henson PM, Fadok VA. Interaction between phosphatidylserine and the phosphatidylserine receptor inhibits immune responses in vivo. J Immunol. 2005; 174:1393–1404. [PubMed: 15661897]
15. Hoffmann PR, Gurary A, Hoffmann FW, Jourdan-Le Saux C, Teeters K, Hashimoto AC, Tam EK, Berry MJ. A new approach for analyzing cellular infiltration during allergic airway inflammation. J Immunol Methods. 2007
16. Kamimura D, Bevan MJ. Endoplasmic reticulum stress regulator XBP-1 contributes to effector CD8+ T cell differentiation during acute infection. J Immunol. 2008; 181:5433–5441. [PubMed: 18832700]
17. Liu KQ, Bunnell SC, Gurniak CB, Berg LJ. T cell receptor-initiated calcium release is uncoupled from capacitative calcium entry in Itk-deficient T cells. J Exp Med. 1998; 187:1721–1727. [PubMed: 9584150]
18. Verma S, Molina Y, Lo YY, Cropp B, Nakano C, Yanagihara R, Nerurkar VR. In vitro effects of selenium deficiency on West Nile virus replication and cytopathogenicity. Virol J. 2008; 5:66. [PubMed: 18513435]
19. Verma S, Lo Y, Chapagain M, Lum S, Kumar M, Gurjav U, Luo H, Nakatsuka A, Nerurkar VR. West Nile virus infection modulates human brain microvascular endothelial cells tight junction proteins and cell adhesion molecules: Transmigration across the in vitro blood-brain barrier. Virology. 2009; 385:425–433. [PubMed: 19135695]
20. Schomburg L, Schweizer U. Hierarchical regulation of selenoprotein expression and sex-specific effects of selenium. Biochim Biophys Acta. 2009; 1790:1453–1462. [PubMed: 19328222]

21. Dadsetan S, Zakharova L, Molinski TF, Fomina AF. Store-operated Ca2+ influx causes Ca2+ release from the intracellular Ca2+ channels that is required for T cell activation. J Biol Chem. 2008; 283:12512–12519. [PubMed: 18316371]
22. Bach TL, Chen QM, Kerr WT, Wang Y, Lian L, Choi JK, Wu D, Kazanietz MG, Koretzky GA, Zigmond S, Abrams CS. Phospholipase cbeta is critical for T cell chemotaxis. J Immunol. 2007; 179:2223–2227. [PubMed: 17675482]
23. McNeill E, Conway SJ, Roderick HL, Bootman MD, Hogg N. Defective chemoattractant-induced calcium signalling in S100A9 null neutrophils. Cell Calcium. 2007; 41:107–121. [PubMed: 16814379]
24. Zemann B, Urtz N, Reuschel R, Mechtcheriakova D, Bornancin F, Badegruber R, Baumruker T, Billich A. Normal neutrophil functions in sphingosine kinase type 1 and 2 knockout mice. Immunol Lett. 2007; 109:56–63. [PubMed: 17292973]
25. Braun A, Gessner JE, Varga-Szabo D, Syed SN, Konrad S, Stegner D, Vogtle T, Schmidt RE, Nieswandt B. STIM1 is essential for Fcgamma receptor activation and autoimmune inflammation. Blood. 2009; 113:1097–1104. [PubMed: 18941110]
26. Zhou X, Yang W, Li J. Ca2+- and protein kinase C-dependent signaling pathway for nuclear factor-kappaB activation, inducible nitric-oxide synthase expression, and tumor necrosis factor-alpha production in lipopolysaccharide-stimulated rat peritoneal macrophages. J Biol Chem. 2006; 281:31337–31347. [PubMed: 16923814]
27. Diamond MS. Virus and host determinants of West Nile virus pathogenesis. PLoS Pathog. 2009; 5 e1000452.
28. Kryukov GV, Kumar RA, Koc A, Sun Z, Gladyshev VN. Selenoprotein R is a zinc-containing stereo-specific methionine sulfoxide reductase. Proc Natl Acad Sci U S A. 2002; 99:4245–4250. [PubMed: 11929995]
29. Tsien RY, Pozzan T, Rink TJ. T-cell mitogens cause early changes in cytoplasmic free Ca2+ and membrane potential in lymphocytes. Nature. 1982; 295:68–71. [PubMed: 6799829]
30. Quintana A, Griesemer D, Schwarz EC, Hoth M. Calcium-dependent activation of T-lymphocytes. Pflugers Arch. 2005; 450:1–12. [PubMed: 15806400]
31. Feske S, Giltnane J, Dolmetsch R, Staudt LM, Rao A. Gene regulation mediated by calcium signals in T lymphocytes. Nat Immunol. 2001; 2:316–324. [PubMed: 11276202]
32. Lewis RS. Calcium signaling mechanisms in T lymphocytes. Annu Rev Immunol. 2001; 19:497–521. [PubMed: 11244045]
33. Parekh AB, Penner R. Store depletion and calcium influx. Physiol Rev. 1997; 77:901–930. [PubMed: 9354808]
34. Putney JW Jr, Broad LM, Braun FJ, Lievremont JP, Bird GS. Mechanisms of capacitative calcium entry. J Cell Sci. 2001; 114:2223–2229. [PubMed: 11493662]
35. Ikura M. Calcium binding and conformational response in EF-hand proteins. Trends Biochem Sci. 1996; 21:14–17. [PubMed: 8848832]
36. Maurer P, Hohenester E. Structural and functional aspects of calcium binding in extracellular matrix proteins. Matrix Biol. 1997; 15:569–580. discussion 581. [PubMed: 9138289]
37. Park CY, Hoover PJ, Mullins FM, Bachhawat P, Covington ED, Raunser S, Walz T, Garcia KC, Dolmetsch RE, Lewis RS. STIM1 clusters and activates CRAC channels via direct binding of a cytosolic domain to Orai1. Cell. 2009; 136:876–890. [PubMed: 19249086]
38. Kaneko T, Li L, Li SS. The SH3 domain--a family of versatile peptide- and protein-recognition module. Front Biosci. 2008; 13:4938–4952. [PubMed: 18508559]
39. Jurynec MJ, Xia R, Mackrill JJ, Gunther D, Crawford T, Flanigan KM, Abramson JJ, Howard MT, Grunwald DJ. Selenoprotein N is required for ryanodine receptor calcium release channel activity in human and zebrafish muscle. Proc Natl Acad Sci U S A. 2008
40. Ye Y, Shibata Y, Yun C, Ron D, Rapoport TA. A membrane protein complex mediates retro-translocation from the ER lumen into the cytosol. Nature. 2004; 429:841–847. [PubMed: 15215856]
41. Klein RS, Diamond MS. Immunological headgear: antiviral immune responses protect against neuroinvasive West Nile virus. Trends Mol Med. 2008; 14:286–294. [PubMed: 18539532]

42. Samuel MA, Diamond MS. Pathogenesis of West Nile Virus infection: a balance between virulence, innate and adaptive immunity, and viral evasion. J Virol. 2006; 80:9349–9360. [PubMed: 16973541]

43. Shrestha B, Diamond MS. Role of CD8+ T cells in control of West Nile virus infection. J Virol. 2004; 78:8312–8321. [PubMed: 15254203]

44. Diamond MS, Shrestha B, Marri A, Mahan D, Engle M. B cells and antibody play critical roles in the immediate defense of disseminated infection by West Nile encephalitis virus. J Virol. 2003; 77:2578–2586. [PubMed: 12551996]

45. Baum MK, Shor-Posner G, Lai S, Zhang G, Lai H, Fletcher MA, Sauberlich H, Page JB. High risk of HIV-related mortality is associated with selenium deficiency. J Acquir Immune Defic Syndr Hum Retrovirol. 1997; 15:370–374. [PubMed: 9342257]

46. Beck MA, Nelson HK, Shi Q, Van Dael P, Schiffrin EJ, Blum S, Barclay D, Levander OA. Selenium deficiency increases the pathology of an influenza virus infection. Faseb J. 2001; 15:1481–1483. [PubMed: 11387264]

47. Beck MA, Levander OA, Handy J. Selenium deficiency and viral infection. J Nutr. 2003; 133:1463S–1467S. [PubMed: 12730444]

48. Yu L, Sun L, Nan Y, Zhu LY. Protection from H1N1 Influenza Virus Infections in Mice by Supplementation with Selenium: A Comparison with Selenium-Deficient Mice. Biol Trace Elem Res.

Abbreviations used

BMDM	bone marrow-derived macrophages
CRAC	calcium release-activated Ca^{2+}
ER	endoplasmic reticulum
KO	knockout
RyR	ryanodine receptor
SDF-1	stromal cell-derived factor 1
Se	selenium
Sel K	selenoprotein K
SOCE	store-operated Ca^{2+} entry
WNV	West Nile virus
WT	wild-type

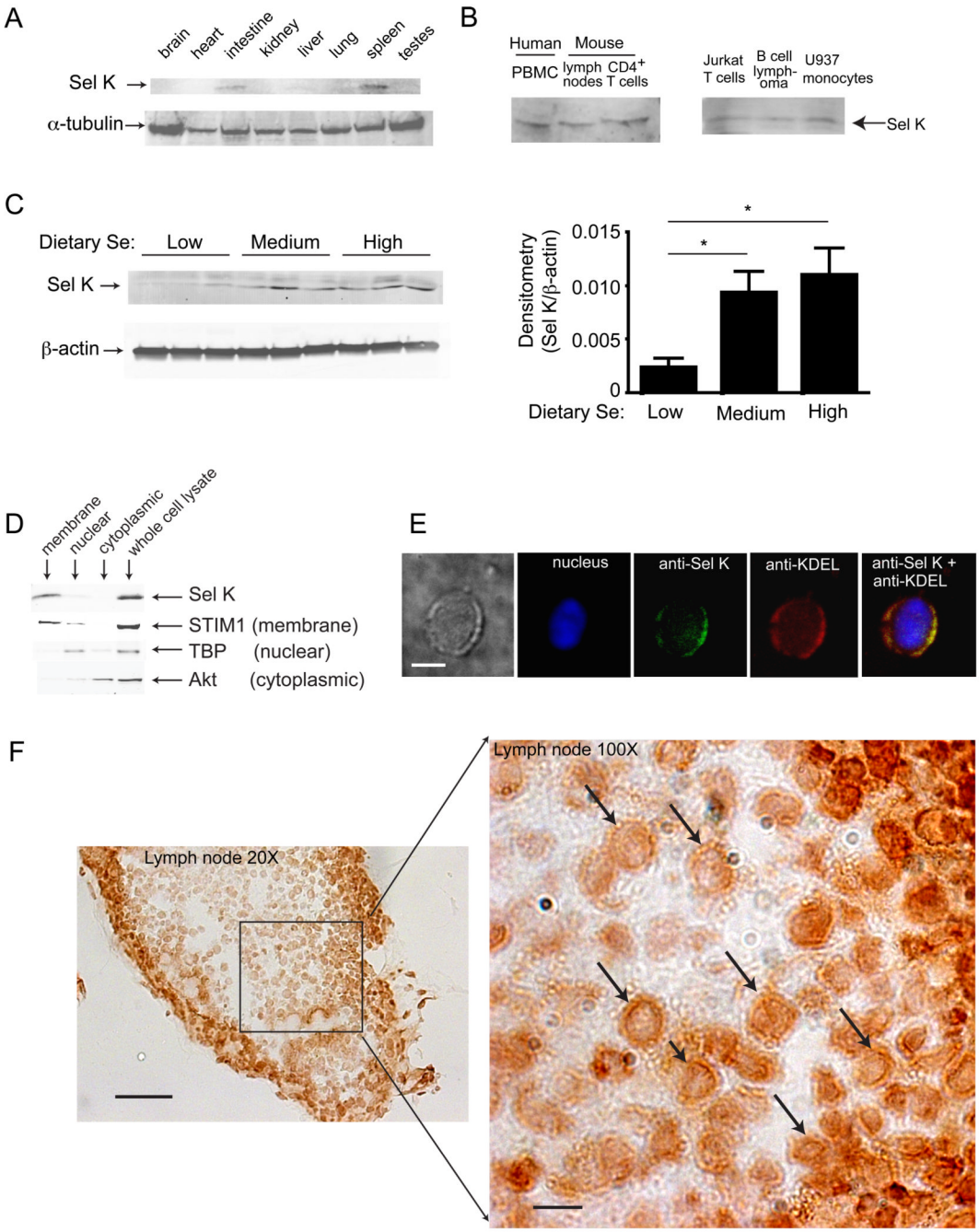

Figure 1.

Characterization of Sel K expression in mouse and human tissues. (A) Western blot analysis of lysates from eight different mouse tissues revealed relatively high levels of Sel K in spleen. Note that α-tubulin was used as a loading control because β-actin is not expressed in the heart. (B) Western blot demonstrated that Sel K is detectable in different primary immune cells (left panel) and cell lines (right panel). (C) Western blots were performed on spleen cells from mice fed low (0.08 ppm), medium (0.25 ppm), and high (1.0 ppm) Se diets and densitometry was performed comparing signal for Sel K/β-actin. Results are expressed as means ± SEM with N= 3 per dietary group. *, $P < 0.05$ using the Students *t* test. (D) Fractionation of Jurkat T cell lysates showed that Sel K is detected in the membrane

fraction. Markers for each fraction included STIM1 for membrane, TBP for nucleus, and Akt for cytoplasm. (E) Primary human lymphocytes were isolated from PBMC and analyzed by immunofluorescence microscopy to detect Sel K, which co-localized with the ER marker, KDEL. Bar, 5 μm. (F) Immunohistochemistry performed on frozen mouse lymph node tissue revealed perinuclear Sel K staining consistent with ER localization (arrows). Bars, 100 μm for 20X image and 10 μm for 100X image. Note that the darker stain around the edges was an artifact of tissue folding and images for pre-immune negative controls are shown in Fig. S3.

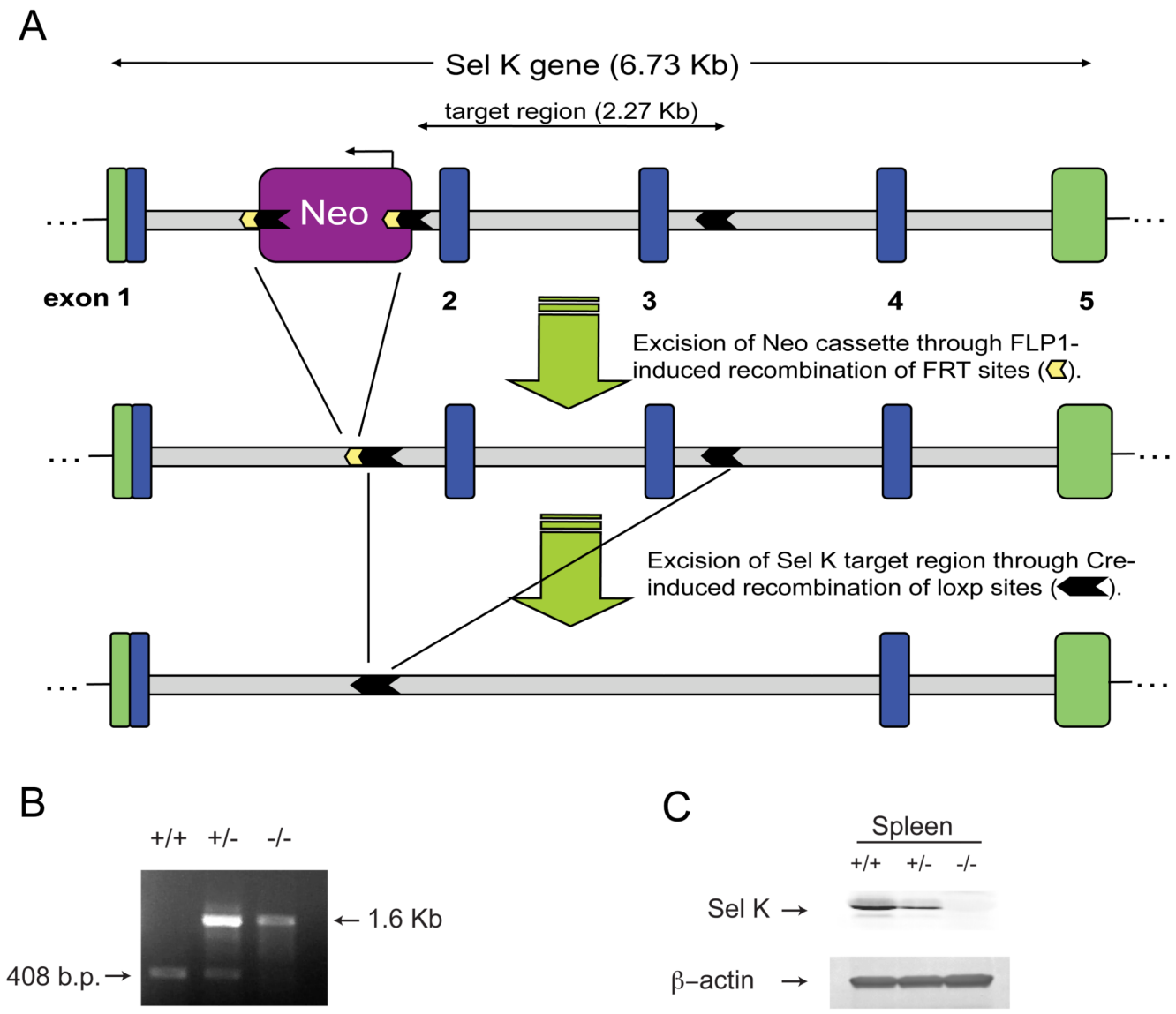

Figure 2.

Generation of Sel K-deficient mice. (A) The mouse Sel K locus on chromosome 14 contains 5 exons, consisting of translated (blue) and untranslated (green) regions. A neomycin-encoding cassette (Neo) was inserted between exons 1 and 2. The Neo cassette was excised through recombination of the two FRT sites (yellow block arrows) by breeding with an FLP-recombinase transgenic mouse. Presence of the LoxP sites (black block arrows) flanking exons 2 and 3 allowed excision of the 2.27 Kb target region by expression of Cre recombinase under control of the CMV promoter. (B) PCR genotyping of mice was performed to detect presence of targeting region in WT allele (408 b.p.) or excision of targeting region in KO allele (1.6 Kb) using primers as described in Methods section. (C) Western blot analysis of spleens from Sel $K^{+/+}$, Sel $K^{+/-}$, and Sel $K^{-/-}$ mice indicated complete deletion of Sel K in homozygous knockout mice.

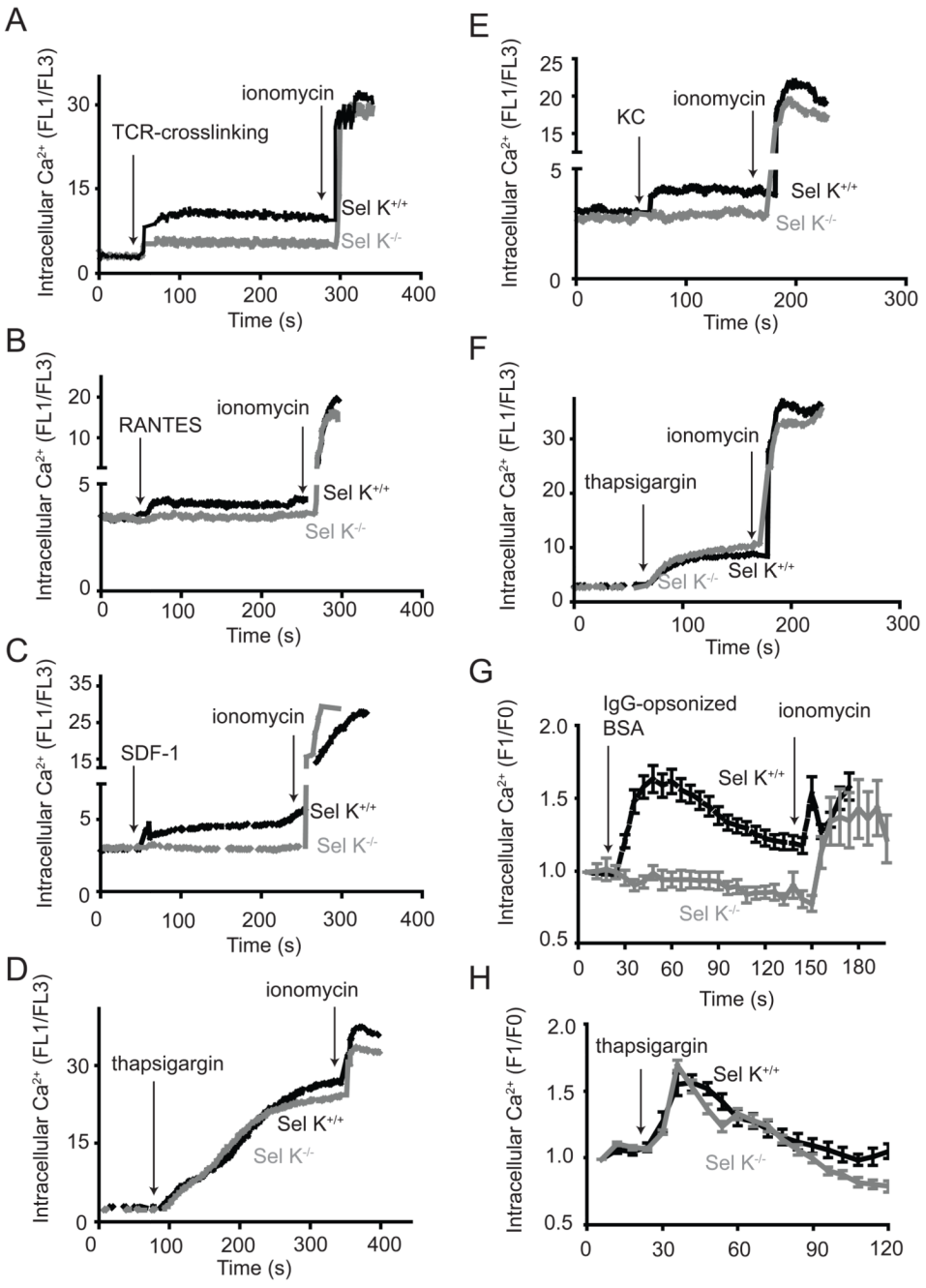

Figure 3.

Receptor-induced Ca^{2+} flux is reduced in T cells, neutrophils, and macrophages from Sel $K^{-/-}$ mice. T cells loaded with Fluo3 and FuraRed were analyzed for FL-1/FL-3 ratio for 1 min and then were stimulated with anti-CD3 (A), RANTES (B), SDF-1 (C), or thapsigargin (D). Ionomycin was added for the last 30 s to confirm equivalent response to this Ca^{2+} ionophore. Neutrophils were analyzed for Ca^{2+} flux in a similar manner as described above for T cells, with stimulation including KC-treatment (E) and thapsigargin-treatment (F). For (A–F), results are representative of three independent experiments. Ca^{2+} flux was measured in BMDM using live-cell, confocal fluorescent microscopy to analyze the ratio of fluo4 fluorescence (F1) to baseline fluo4 fluorescence (F0) with stimulation by addition of IgG-

opsonized BSA (G) or thapsigargin (H). For (G-H), fluorescence was measured for a minimum of 25 cells per group for each experiment with results expressed as means ± SEM for three independent experiments

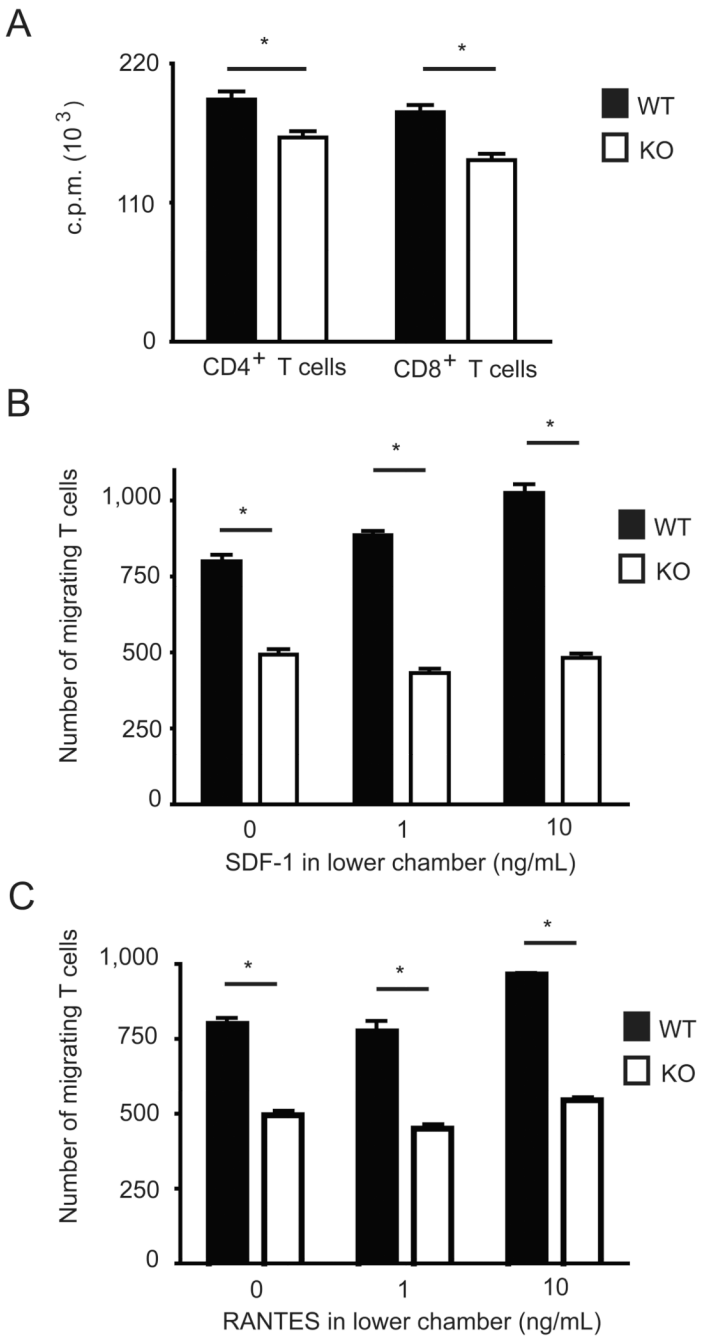

Figure 4.

Ca^{2+}-dependent functions are reduced in T cells from Sel $K^{-/-}$ mice. (A) Both $CD4^+$ and $CD8^+$ T cells exhibited significantly reduced proliferation when cultured in anti-CD3/CD28-coated plates for 72 h. Migration assays were performed using pan T cells purified from spleen and added to transwell plates with 0, 1, or 10 ng/mL SDF-1 (B) or RANTES (C) added to the lower chamber. Results are expressed as means ± SEM for triplicates and representative of two independent experiments. *, $P < 0.05$ using the Students *t* test.

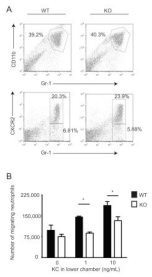

Figure 5.

Chemotaxis is reduced in neutrophils from Sel $K^{-/-}$ mice. (A) Percent of bone marrow cells expressing neutrophil markers ($Gr\text{-}1^{+}CD11b^{+}$) were similar for WT and Sel $K^{-/-}$ mice and expression of the chemokine receptor that binds KC, CXCR2, was similar for neutrophils from WT and Sel $K^{-/-}$ mice. (B) Migration assays were performed using neutrophils purified from bone marrow and added to transwell plates with 0, 1, or 10 ng/mL KC added to the lower chamber. Results are expressed as means ± SEM for triplicates and representative of two independent experiments. *, $P < 0.05$ using the Students *t* test.

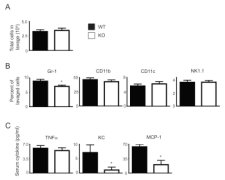

Figure 6.

Decreased neutrophil infiltration and chemokine secretion are exhibited during peritonitis in Sel $K^{-/-}$ mice. (A) Peritonitis was induced in WT and Sel $K^{-/-}$ mice by i.p. injection of the viral mimetic, poly (i:c). After 48 h, total cells in peritoneal lavages were enumerated. (B) Peritoneal lavages were analyzed by four-color flow cytometry to determine percent neutrophils ($Gr\text{-}1^+$), macrophages ($CD11b^+$), dendritic cells ($CD11c^+$), and NK cells ($NK1.1^+$). (C) Three cytokines were detectable in sera from mice at 48 h after induction of peritonitis, including TNFα, KC, and MCP-1. Results are expressed as means ± SEM for six mice per group pooled from two independent experiments. *, $P < 0.05$ using the Students *t* test.

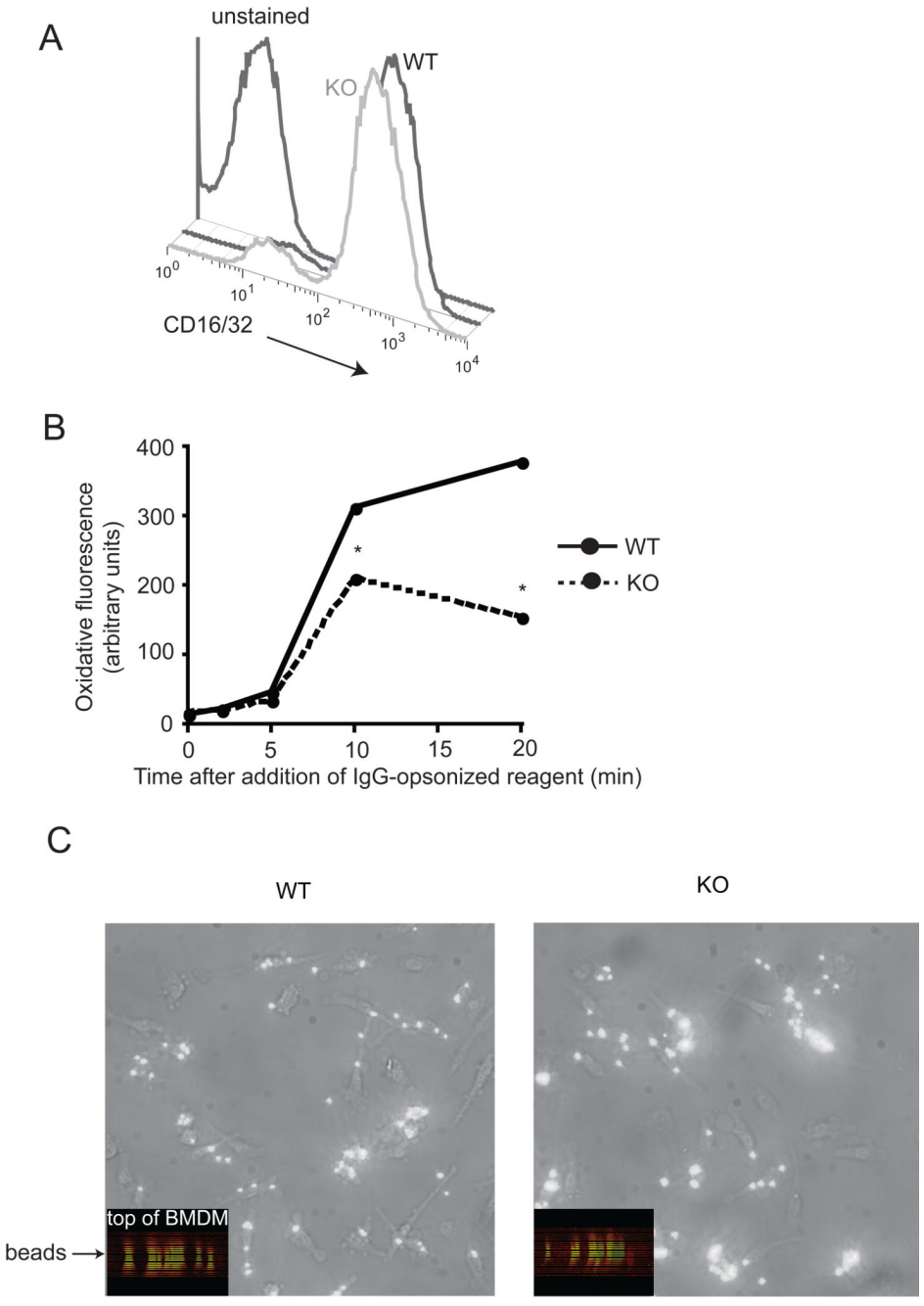

Figure 7.

Fcγ-receptor-mediated oxidative burst is reduced in macrophages from Sel $K^{-/-}$ mice. (A) Bone marrow-derived macrophages were analyzed for expression of high affinity Fcγ-receptors (CD16 and CD32), which were equivalent between WT and Sel $K^{-/-}$ mice. (B) Oxidative burst generated during Fcγ-receptor-mediated phagocytosis of IgG-opsonized complexes was significantly reduced in macrophages from Sel $K^{-/-}$ mice compared to WT controls. Results are expressed as means ± SEM for triplicates representative of two independent experiments. Note that SEM bars are present in (B), but do not appear due to their small size in comparison to Y values. *, $P < 0.05$ using the Students *t* test. (C) Phagocytosis of 1 μm diameter polystyrene beads was similar between WT and KO. Bars,

20 μm. Inserts display 3-D rendering of Z-stack images confirming complete ingestion of beads (green) between plasma membrane (red) was similar between WT and KO BMDM.

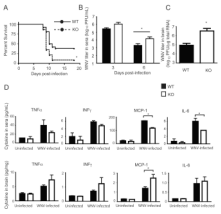

Figure 8.

Sel $K^{-/-}$ mice fail to effectively clear WNV and exhibit increased WNV-induced mortality. (A) Mice were inoculated 10^2 PFU WNV in footpads and monitored for survival over 18 d (N = 26 for WT, N = 23 for KO). Data were obtained from two independent experiments and pooled. *, P < 0.05 using the Kaplan-Meier log-rank test. (B) WNV plaque assays were performed on sera from 3 and 6 d post-infection (N = 14 for WT, N = 13 for KO). Data were obtained from two independent experiments and pooled. *, P < 0.05 using the Students *t* test. (C) Real-time qRT-PCR was used to evaluate WNV mRNA in whole brain from mice sacrificed 7 d post-infection (N = 6 for WT, N = 7 for KO). Data represent two independent experiments with each sample analyzed in duplicate. *, P < 0.05 using a Mann-Whitney test. (D) Cytokines were measured in sera (day 6) or whole brain lysates (day 7) and results are expressed as means ± SEM (N = 3). *, P < 0.05 using the Students *t* test.

Table I

Lymphocyte Numbers in Lymphoid Tissues

		$CD4^+$ thymocytes (10^6)	$CD8^+$ thymocytes (10^6)	$CD4^+CD8^+$ thymocytes (10^6)
Thymus	WT	1.86 ± 0.58	0.64 ± 0.05	24.3 ± 0.04
	KO	1.98 ± 0.76	0.71 ± 0.04	22.4 ± 0.08
		$CD4^+$ T cells (10^6)	$CD8^+$ T cells (10^6)	$B220^+$ B cells (10^6)
Lymph Node	WT	0.48 ± 0.02	0.38 ± 0.03	0.33 ± 0.05
	KO	0.50 ± 0.008	0.39 ± 0.002	0.34 ± 0.05
		$CD4^+$ T cells (10^6)	$CD8^+$ T cells (10^6)	$B220^+$ B cells (10^6)
Spleen	WT	15.5 ± 0.6	9.85 ± 0.2	43.5 ± 4.3
	KO	15.9 ± 0.5	10.0 ± 1.1	44.6 ± 5.9

Numbers represent mean ± S.E. (N = 5)